

REVIEW PAPER

Image Reconstruction of Simulated Specimens using Convolution Back Projection

Mohd. Farhan Manzoor, Pankaj Yadav, K. Muralidhar and P. Munshi

Indian Institute of Technology, Kanpur - 208 016

ABSTRACT

This paper reports about the reconstruction of cross-sections of composite structures. The convolution back projection (CBP) algorithm has been used to capture the attenuation field over the specimen. Five different test cases have been taken up for evaluation. These cases represent varying degrees of complexity. In addition, the role of filters on the nature of the reconstruction errors has also been discussed. Numerical results obtained in the study reveal that CBP algorithm is a useful tool for qualitative as well as quantitative assessment of composite regions encountered in engineering applications.

Keywords: Convolution back projection, computerised tomography, simulated specimens, error analysis

1. INTRODUCTION

Composite materials are playing an increasingly crucial role in several industries. Continuous effort is being made to manufacture improved composites for specific applications. Non-destructive testing (NDT) using computerised tomography (CT) is an important methodology in routine inspection of material samples.

With the advent of high resolution CT scanners, it is possible to image cross-section with a pixel size¹ of 20 μm . Following Herman², one can define tomography as image reconstruction from projections which is a process of producing an image of a two-dimensional distribution usually of some physical property from its path integral. Convolution back projection (CBP) and algebraic reconstruction technique (ART) are two types of algorithms by which tomographic inversion can be implemented. In the present work, the CBP has been chosen as the tomographic algorithm in view of its established convergence properties. The projection data constitutes

the input for the CBP calculation. In experiments, it is calculated for the cross-section to be reconstructed using X-ray and γ -ray sources. To gain experience with CBP, it is not necessary to conduct laboratory experiment. Instead, the projection data can be calculated mathematically for geometrically simulated specimens. The experience with CBP to non-destructive evaluation of various such specimens is reported in the present study.

2. THEORETICAL BACKGROUND

The computational and mathematical procedures underlying the data collection, image reconstruction and image display used in the CT are discussed here.

2.1 Preliminary Studies

Tomographic inversion using X-rays and γ -rays is based on the attenuation of the radiation intensity as it passes through the solid material being tested. The number of photon counts after passing along a curve C in the material is given by

$$N = N_0 \exp \left[- \int_C \mu(r, \phi) dl \right] \quad (1)$$

where the integration is along the chord length of C , N is the number of photon counts after traversing the chord length, N_0 is the initial photon counts and μ is the attenuation coefficient. Since μ depends on the material and the energy of the radiation, a distribution of μ is a direct indicator of the material composition of the component being studied. For the present study, the radiation source has been taken to be monoenergetic and the dependence of μ on the material structure alone has been included. Equation (1) can be written as

$$\ln \left(\frac{N}{N_0} \right) = \int_C \mu(r, \phi) dl = p(s, \theta) \quad (2)$$

where $p(s, \theta)$ is called the projection data for the tomographic algorithm. It is the integral of the function along the line specified by s and θ . Figure 1 explains the symbols r , ϕ , s and θ .

The aim of tomography is to reconstruct the function $\mu(r, \phi)$ if a set of several values of $p(s, \theta)$ measured along various chords (C) is given. The CBP algorithm has been used for this reconstruction. The μ values can be suitably normalised to get the material density distribution.

2.2 Data Collection Mode

The image processing methodology requires attenuation data to be collected by an array of radiation detectors for the reconstruction of the function $\mu(r, \phi)$. In the present study, the mode of collection is the parallel beam geometry, as shown in Fig. 1. This system consists of several pairs of radiation sources and radiation detectors, which can scan the object completely. SD (source-detector) pairs are spaced uniformly and the object can be rotated to get the data for different views. The line SD represents the path of the data ray or the chord along which the function $p(s, \theta)$ can be found. The perpendicular distance from the centre of the object to the path of the ray is denoted by s . The object table is rotated to get several sets of p for

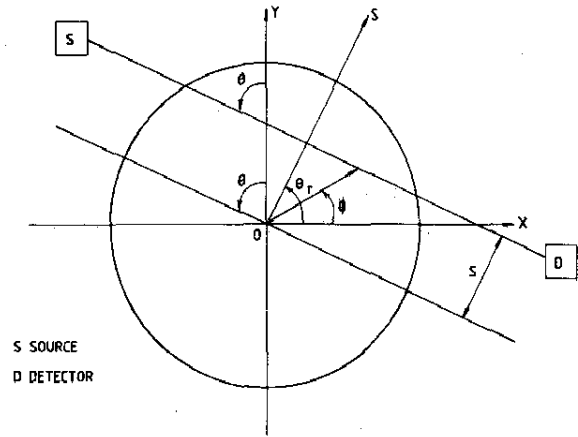


Figure 1. Data collection geometry for CBP-based CT scanner

different values of q . Typical values of the number of rays and the number of projections used are 100 and 100. The source-detector system is moved pixel by pixel, thus generating a grid of 100 × 100 over the physical region of interest.

A second configuration used for data collection in applications is the fan beam geometry. It comprises a single source and multiple detectors. It can be shown that the fan beam and the parallel beam have a one-to-one geometric relationship and the data recorded in one setup can be mapped to the other without ambiguity.

2.3 Convolution Back Projection Algorithm

CT scanners were developed initially for medical imaging. They have been used in the material evaluation for the past 10 years. A detailed mathematical treatment on this subject is available^{2,3}. For completeness, the salient mathematical features of the CBP algorithm, developed originally by Ramachandran and Laxminarayanan⁴ are reported.

Figure 1 shows the data collection geometry for a parallel beam CT scanner. The object function to be reconstructed is the attenuation coefficient $\mu(r, \phi)$, and more generally identified by $f(r, \phi)$, to indicate other physical properties, such as density, void fraction and refractive index. The object is represented by a unit circle and one (of the many) data ray is represented by SD. The ray indices are s and θ , where s is the perpendicular distance of the ray from the object centre, and θ is the angle of the source position (or object rotation). CT data denoted by $p(s, \theta)$ is given by

be the highest frequency contained in \hat{p} . In general, to avoid aliasing artifacts, the choice, $R_c = 1/(2\Delta s)$ is recommended. Here, Δs is the spacing between the data rays.

It has been shown by Munshi⁵⁻⁷, *et al.* that E_1 at a given point (r, ϕ) in the object cross-section is given by:

$$E_1(r, \phi) \approx k[W''(0)][\nabla^2 f(r, \phi)] \quad (13)$$

where

$$W''(0) = \left. \frac{\partial^2 W(R)}{\partial R^2} \right|_{R=0} \quad (14)$$

where $\nabla^2 f$ is the Laplacian of f , and k is a constant depending on the data ray spacing.

Equation (13), the first Kanpur theorem for errors in CBP is valid for objects having certain smoothness properties provided the data is perfect as per Eqn (3). The error E_1 represents the point-wise theoretical error in the reconstruction, and it is also obvious that the Laplacian of $f(r, \phi)$ has to exist for the predictions of the theorem to be valid. For points in the cross-section, where $\nabla^2 f$ does not exist, the linearity between E_1 and $W''(0)$ is disturbed. If $\nabla^2 f$ is zero or near zero, other errors will be more dominant. The Laplacian is zero for smooth regions of the objects, while it does not exist for rough edges¹.

For simulated objects, E_1 can be calculated with reference to the original image. For real objects, the distribution is unknown, hence the error in reconstruction cannot be calculated directly. This fact motivates an indirect representation of error. It has been reported earlier that, for a given data set, sharpness can be used as an indicator of the error behaviour, arising due to the choice of the filter function.

If the image consists of a single point, then the sharpness parameter is defined as the value of the reconstructed gray level at that point. For a general image, the sharpness parameter corresponds to N_{\max} , the maximum gray level (linear absorption coefficient) in the reconstruction.

Table 1. Details of Hamming filters selected

Filter	B	$ W''(0) $
H54	0.540	0.460
H75	0.750	0.250
H80	0.800	0.200
H91	0.917	0.083
H99	0.999	0.001

3. TEST CASES

The following cross-sections have been taken up for the analysis:

- (a) Unit circle (S1)
- (b) Circular cross-section with one hole at the geometric centre (S2)
- (c) Circular cross-section with four holes at the corners and a large hole at the centre (S3)
- (d) Circular cross-section with a crack (S4)
- (e) Circular cross-section with star-shaped object at the centre and small circular inserts (S5)

With the cross-sections prescribed at each pixel of a predetermined grid, the projection data has been numerically calculated using Eqn (3). Tomographic inversion is then implemented using Eqn (5). In the present study, Hamming filters have been used in Eqn (7). They are given by

$$W(R) = \begin{cases} B+(1-B)\cos(\pi R/R_c) & |R| \leq R_c \\ 0 & |R| > R_c \end{cases} \quad (15)$$

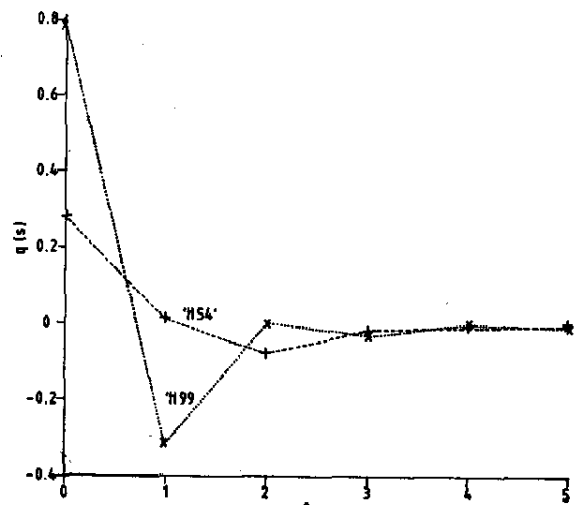


Figure 2. Comparison of H54 and H99 filters

The details of the filter parameter are listed in Table 1 along with their second derivatives in the Fourier-space, $W''(0)$. The plot of s versus $q(s)$ for Hamming 54(smooth) and Hamming 99 (sharp) filter is also given in Fig. 2.

For the purpose of displaying the reconstructed image, the CT numbers are read from the CBP output file and appropriate gray levels assigned corresponding to it. Thus by generating pixels for each of the projection data at their position, the CT image can be graphically displayed.

4. RESULTS & DISCUSSION

The results obtained on tomographic reconstruction have been presented. For each test case, a set of eight images have been included. These are: (i) original cross-section, (ii) a set of vertically stacked projections called the Sinogram, (iii) first projection at an angle $\theta = 0^\circ$ (0° radiograph), (iv) 50^{th} projection at $\theta = 90^\circ$ (ninety degree radiograph), (v) reconstructed cross-section with the H54 filter, (vi) corresponding error image, (vii) reconstructed cross-section with the H99 filter, and (viii) corresponding error image. A quantitative assessment of the errors has also been presented.

4.1 Reconstruction with Simulated Objects

The simulated data derived from the five samples specified earlier have been used for reconstruction

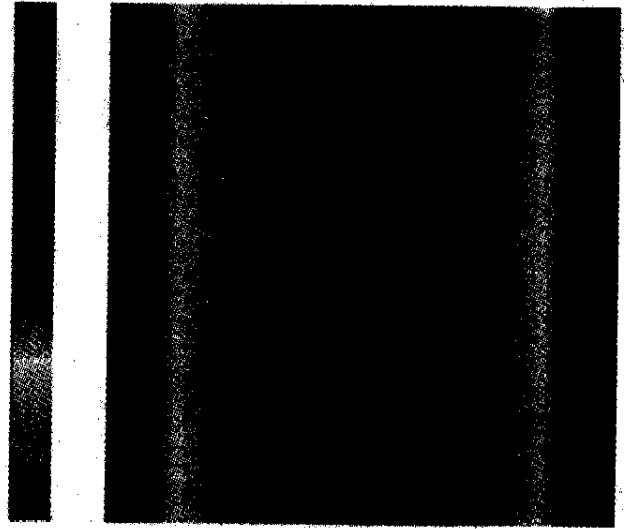


Figure 3(b). Sinogram of S1 with 100 projections vertically stacked.

using the CBP algorithm. The reconstructed images and the error in the reconstructed images are shown in Figs (3) to (7). Reconstruction using both the H54 and H99 filters have been shown. H99 being a sharp filter is able to show the small-scale features in a better way as compared to H54 filter which in turn is smooth.

Examining the reconstructed image, one can conclude that CBP has recovered all the artifacts present in the samples and hence has been successful. The reconstructed gray level distribution is symmetrical for symmetrical objects. It may be noted that the reconstructed images

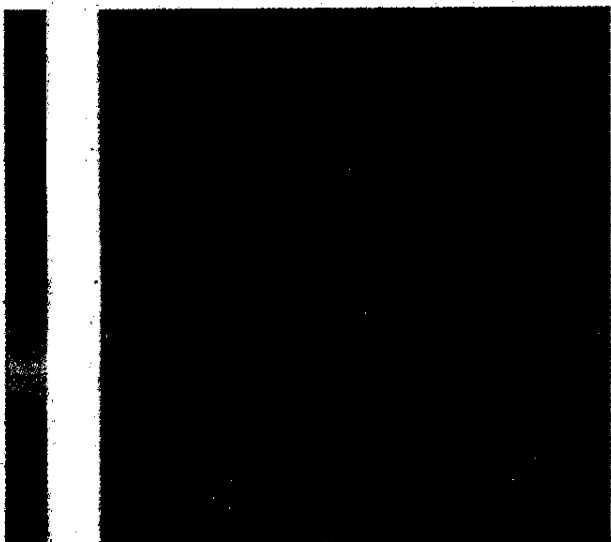


Figure 3(a). Test case S1

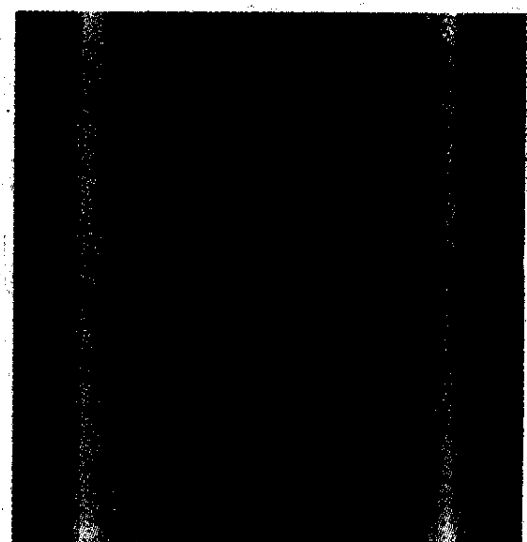


Figure 3(c). Radiograph of S1 for the 1st view



Figure 3(d). Radiograph of S1 for the 50th view

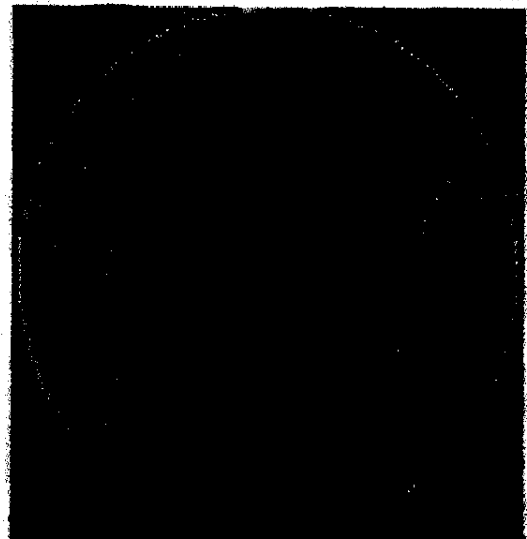


Figure 3(g). Reconstruction of S1 with H99 filter



Figure 3(e). Reconstruction of S1 with H54 filter

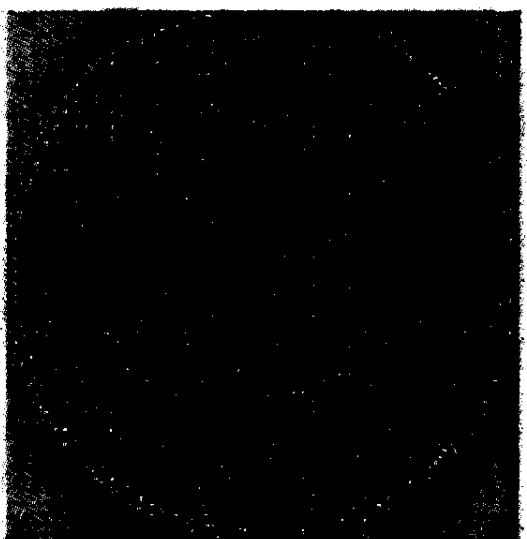


Figure 3(h). Error in S1 with H99 filter

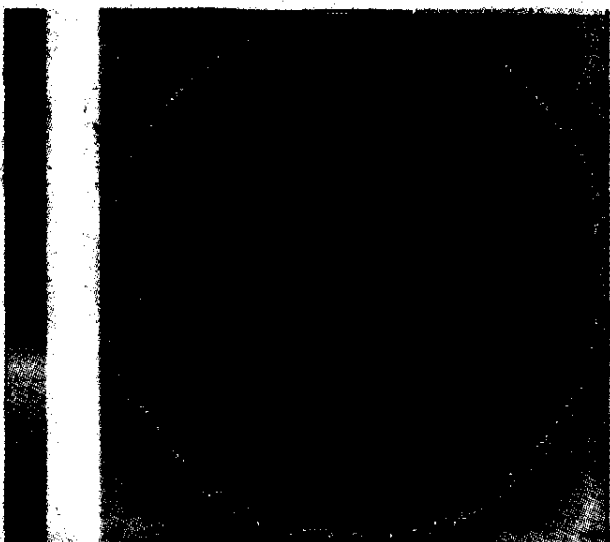


Figure 3(f). Error in S1 with H54 filter

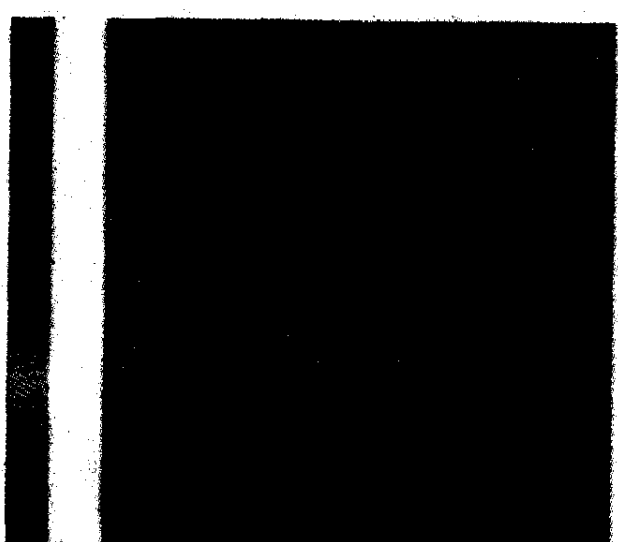


Figure 4(a). Test case S2

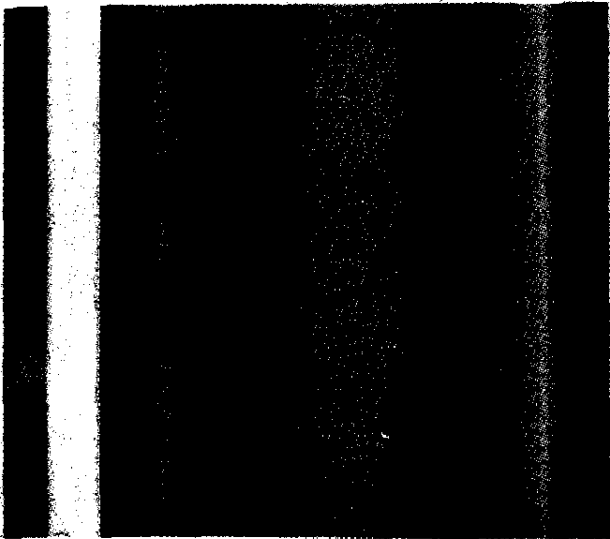


Figure 4(b). Sinogram of S2 with 100 projections vertically stacked.



Figure 4(d). Radiograph of S2 for the 50th view

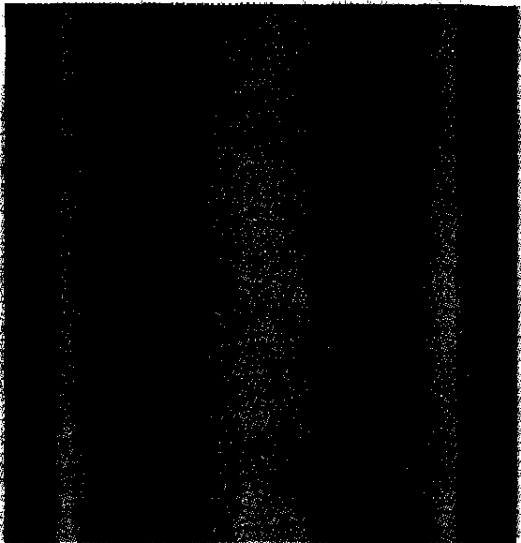


Figure 4(c). Radiograph of S2 for the 1st view

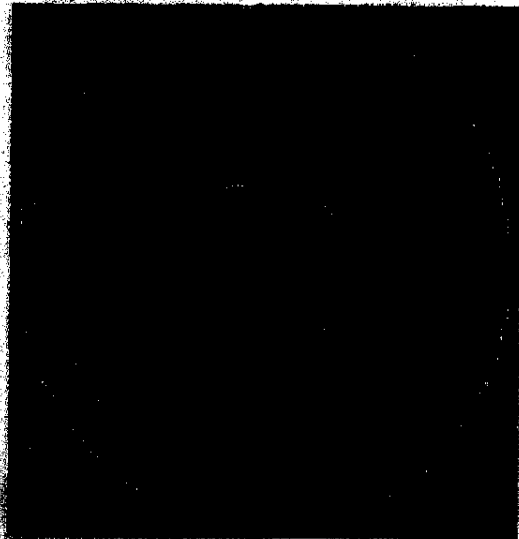


Figure 4(e). Reconstruction of S2 with H54 filter

do not show a sharp change at the edges as in the case for actual objects. The edge effect is visible but the density of the reconstructed sections of simulated data is uniform at 4-6 pixel width away from the edges. From the viewpoint of object identification, this level of accuracy is quite acceptable.

4.2 Error Analysis

Having reconstructed the image, it is important to have some means of measuring the correctness (reliability) of reconstruction. In general, the error



Figure 4(f). Error in S2 with H54 filter

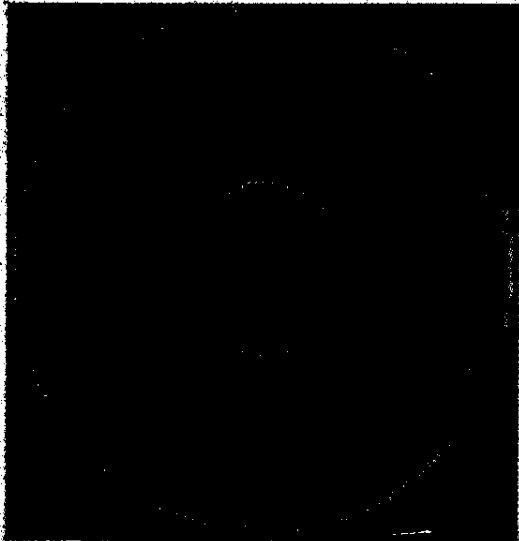


Figure 4(g). Reconstruction of S2 with H99 filter

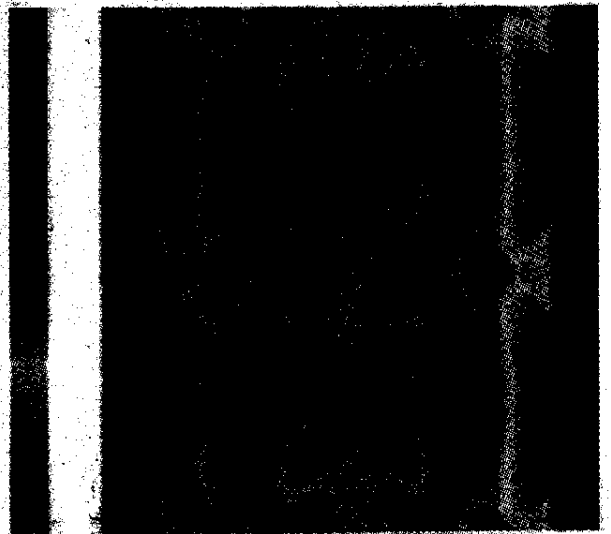


Figure 5(b). Sinogram of S3 with 100 projections vertically stacked.

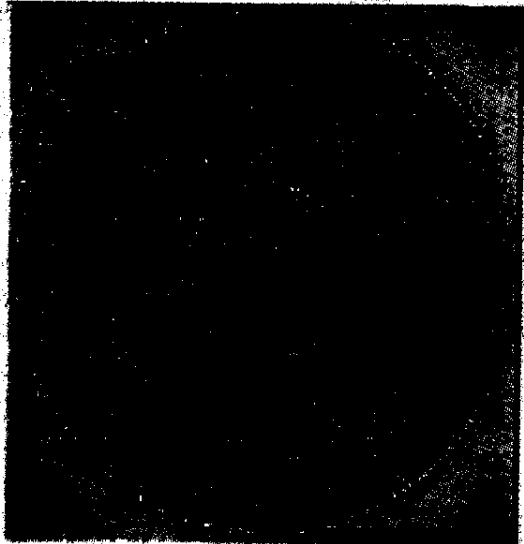


Figure 4(h). Error in S2 with H99 filter

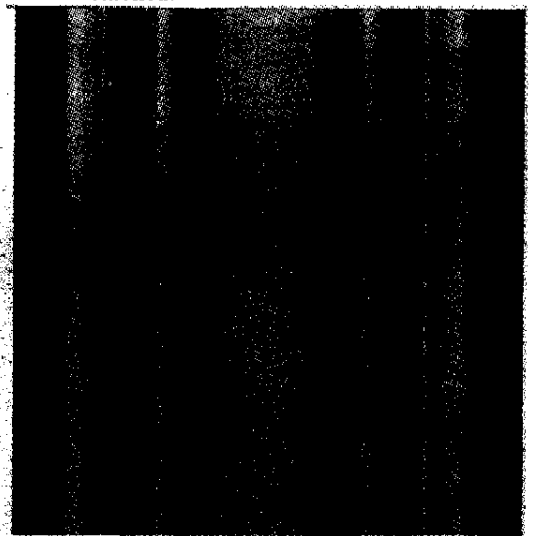


Figure 5(c). Radiograph of S3 for the 1st view

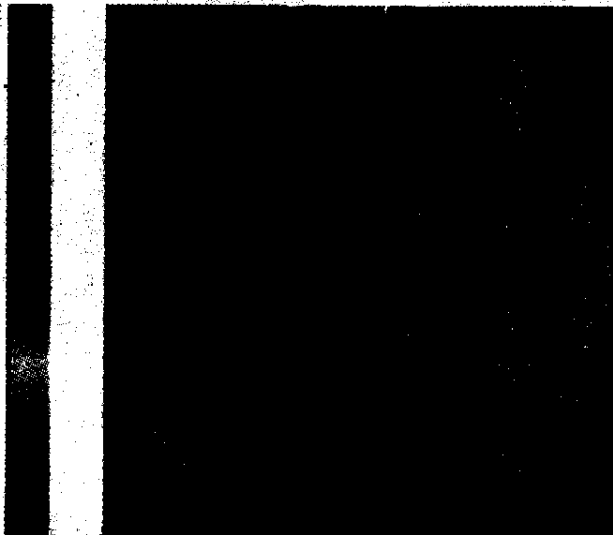


Figure 5(a). Test case S3

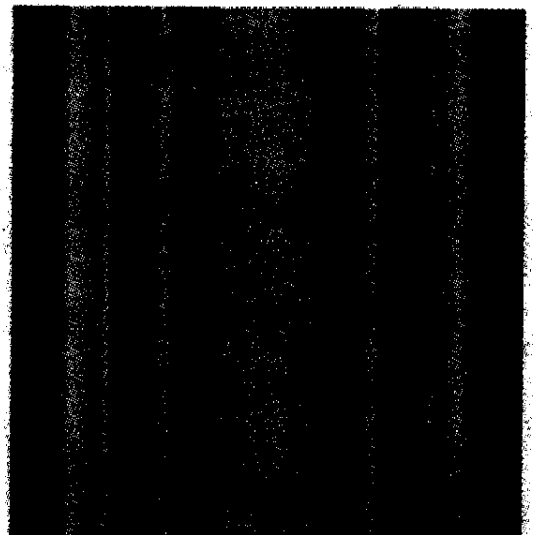


Figure 5(d). Radiograph of S3 for the 50th view

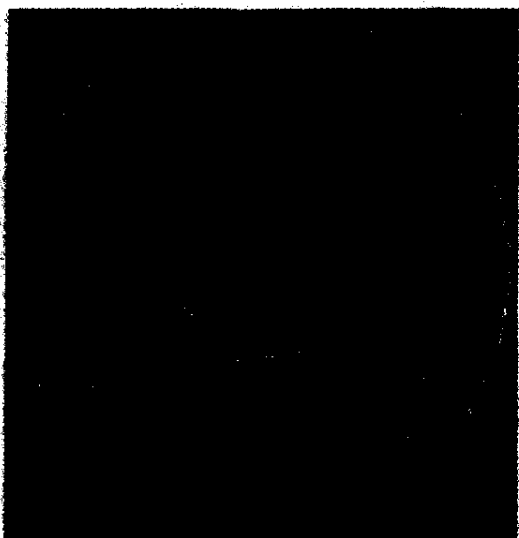


Figure 5(e). Reconstruction of S3 with H54 filter

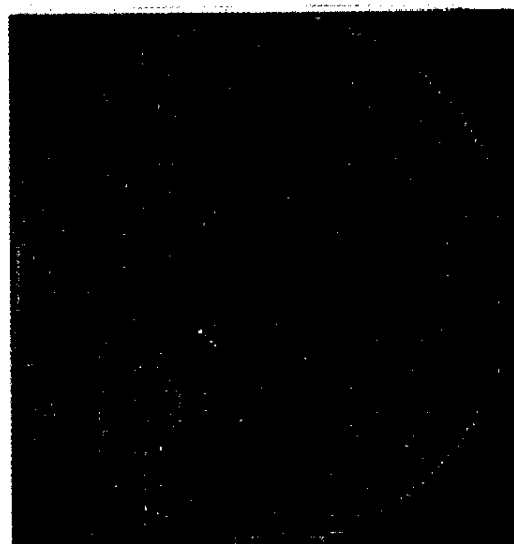


Figure 5(h). Error in S3 with H99 filter

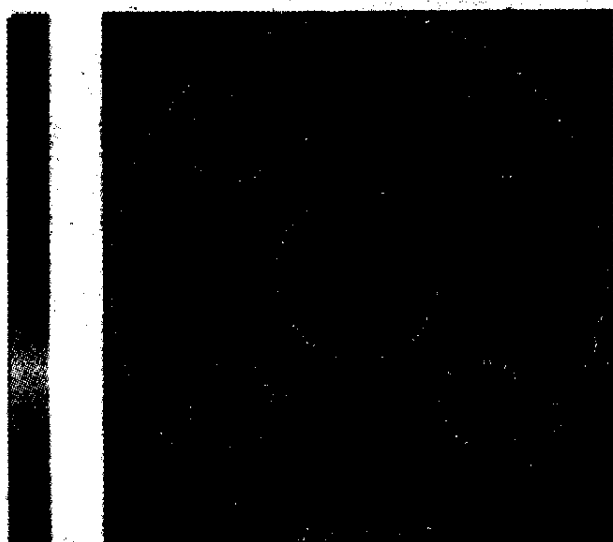


Figure 5(f). Error in S3 with H54 filter

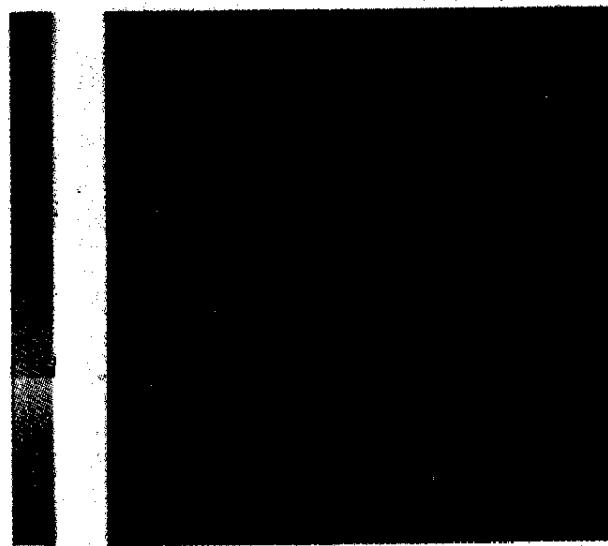


Figure 6(a). Test case S4

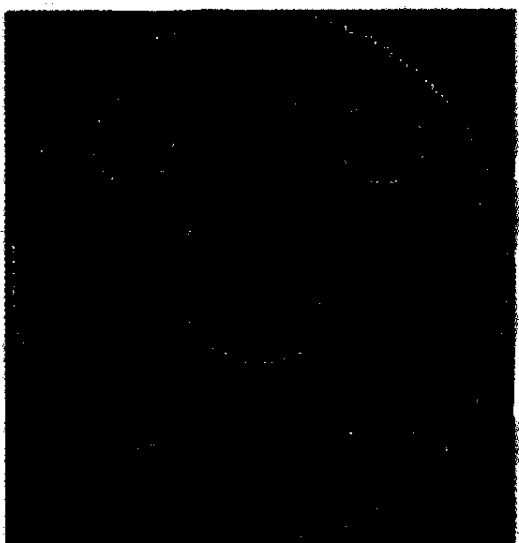


Figure 5(g). Reconstruction of S3 with H99 filter



Figure 6(b). Sinogram of S4 with 100 projections vertically stacked.

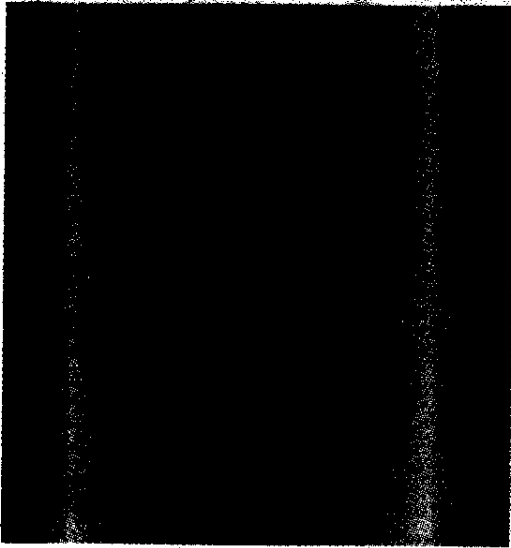


Figure 6(c). Radiograph of S4 for the 1st view

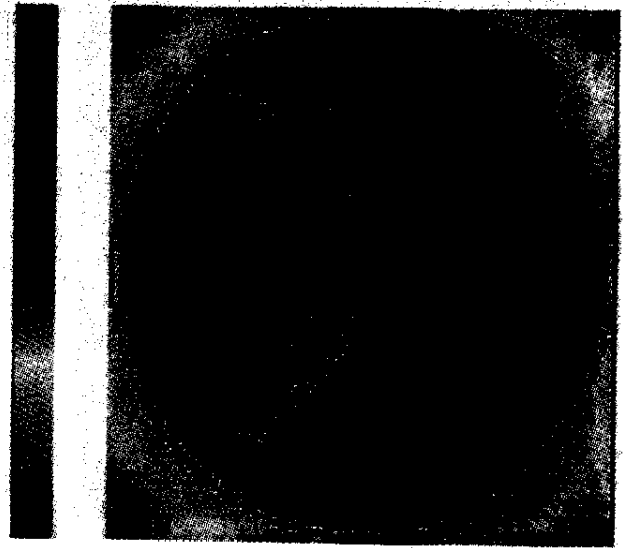


Figure 6(f). Error in S4 with H54 filter

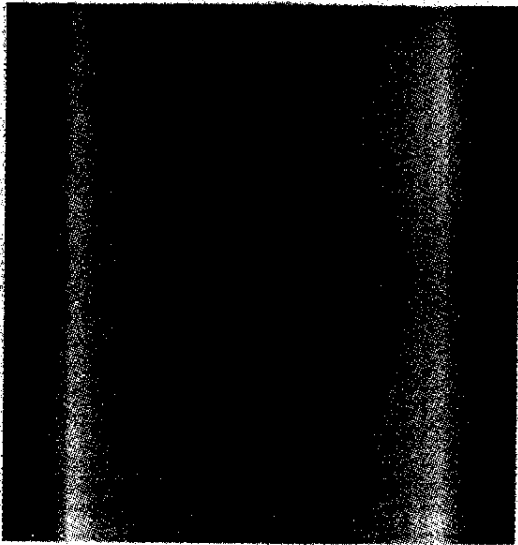


Figure 6(d). Radiograph of S4 for the 50th view

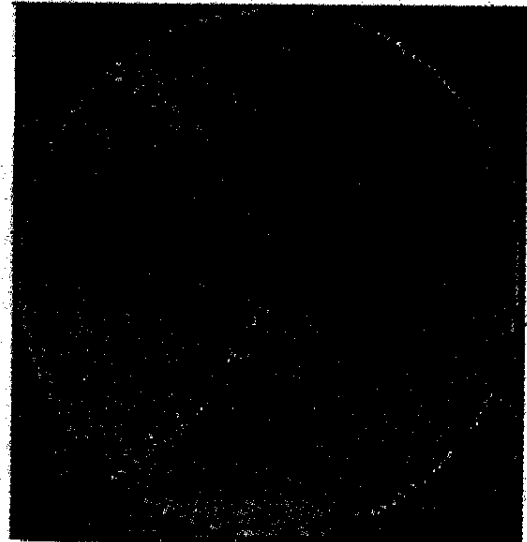


Figure 6(g). Reconstruction of S4 with H99 filter

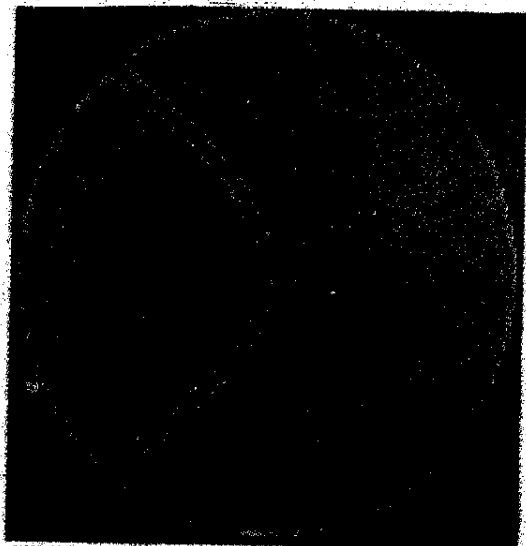


Figure 6(e). Reconstruction of S4 with H54 filter

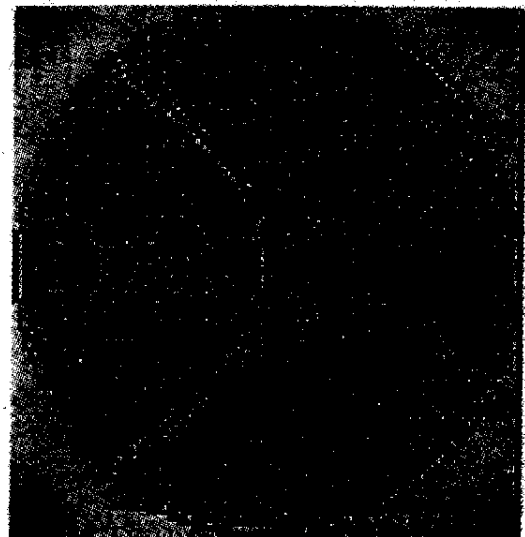


Figure 6(h). Error in S4 with H99 filter

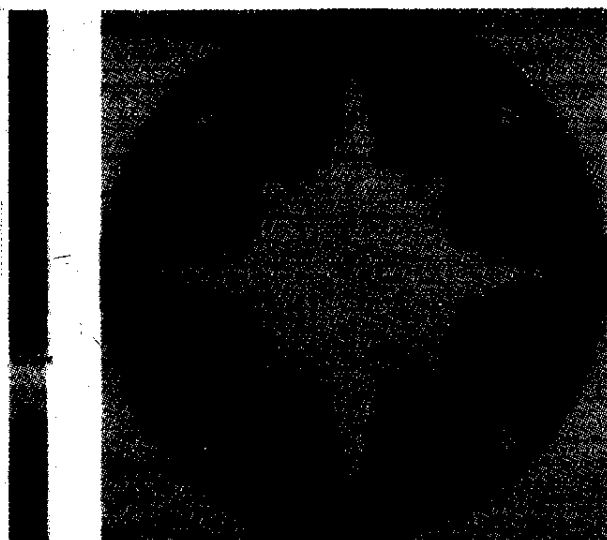


Figure 7(a). Test case S5

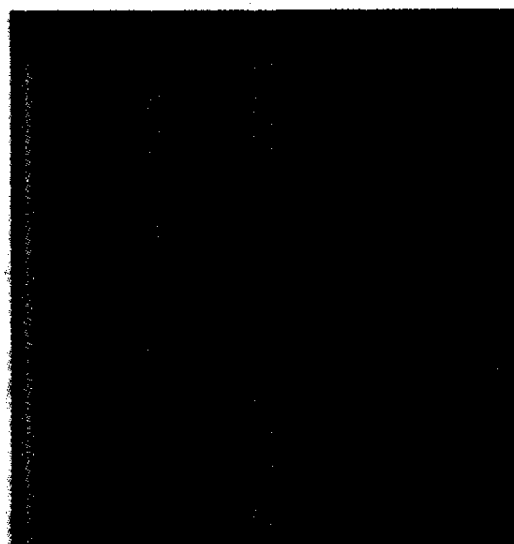


Figure 7(d). Radiograph of S5 for the 50th view

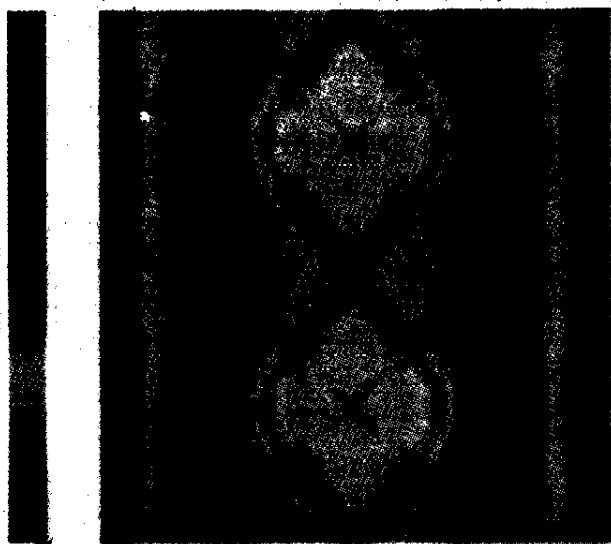


Figure 7(b). Sinogram of S5 with 100 projections vertically stacked.



Figure 7(e). Reconstruction of S5 with H54 filter

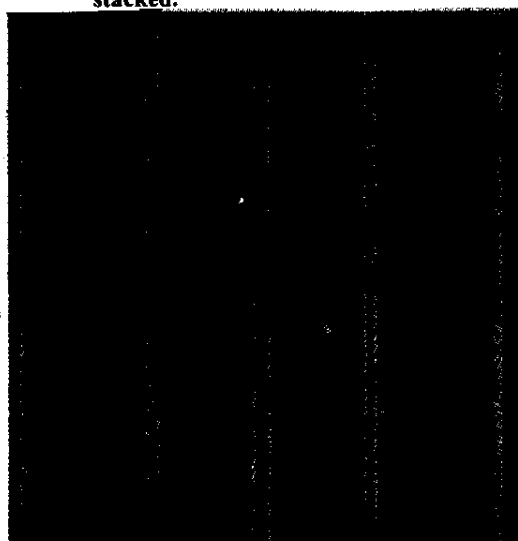


Figure 7(c). Radiograph of S5 for the 1st view

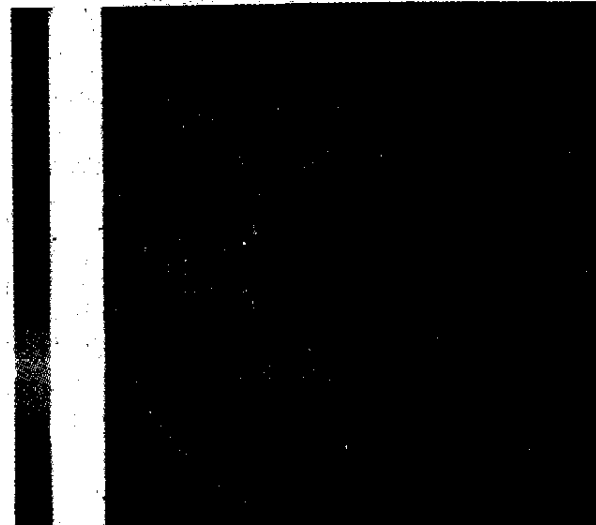


Figure 7(f). Error in S5 with H54 filter



Figure 7(g). Reconstruction of S5 with H99 filter

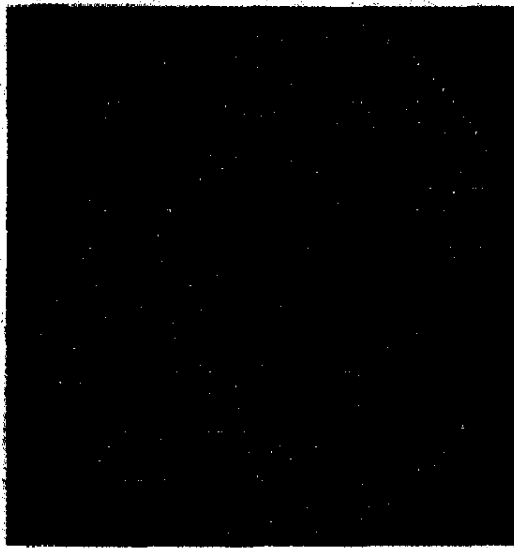


Figure 7(h). Error in S5 with H99 filter

consists of two components⁵. These are error in collecting the data and error in reconstruction algorithm. For simulated data, the first component of the error is absent and the error is entirely due to the second component. For simulated data, error has been calculated by comparing the actual values and reconstruction values of the absorption coefficient pixel-by-pixel. The error images are shown for all specimens with H54 and H99 filters. The first Kanpur error theorem as given by Eqn (13) was also verified for all the specimens. Table 2 shows N_{max} values for different simulated objects.

For a given cross-sectional distribution $f(r, \phi)$ the pointwise error in reconstruction is proportional

Table 2. Summary of results for simulated data for hamming filters

Filter	Specimens				
	S1	S2	S3	S4	S5
	N_{max}	N_{max}	N_{max}	N_{max}	N_{max}
H54	1.032	1.089	1.096	1.102	1.164
H75	1.064	1.112	1.141	1.116	1.191
H80	1.091	1.121	1.151	1.120	1.198
H91	1.155	1.168	1.178	1.168	1.221
H99	1.199	1.213	1.208	1.216	1.251

to the magnitude of $W''(0)$, provided that the collected data are perfect, and the specimen character around the point given in question is such that Eqn (13) is valid⁶. Hence processing of a given data set by several filters results in a linear relationship between $W''(0)$ and E_1 . The plots have been given in Figs 8 and 9. Samples S1, S2 and S3 show wide variation from linearity. Since these samples are smooth, $\nabla^2 f$ vanishes for the major portion of the region and hence Eqn (13) no longer represents the total error in this case. Samples S3 and S4 show a good linear fit because for these samples $\nabla^2 f$ exists (Table 3).

Table 3. Curve-fitting details

Specimens	Goodness of fitness (%)	Reference
S1	2.3540	Figure 8
S2	2.0958	Figure 8
S3	0.5251	Figure 9
S4	2.4847	Figure 9
S5	0.8876	Figure 9

5. CONCLUSIONS

CBP has been used for non-destructive evaluation of composite specimens from their projection data. A class of Hamming filters with varying degrees of smoothness have been used as mathematical filters. The results obtained in the present work lead to the following conclusions:

- (a) It was possible to reconstruct quantitatively all the specimen cross-sections of varying complexity.

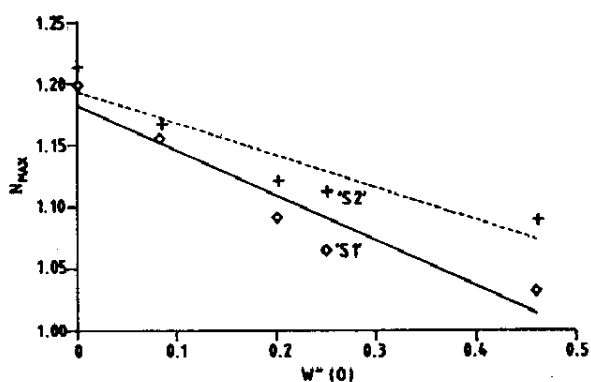


Figure 8. Maximum grey level (N_{max}) plot for test cases S1 and S2.

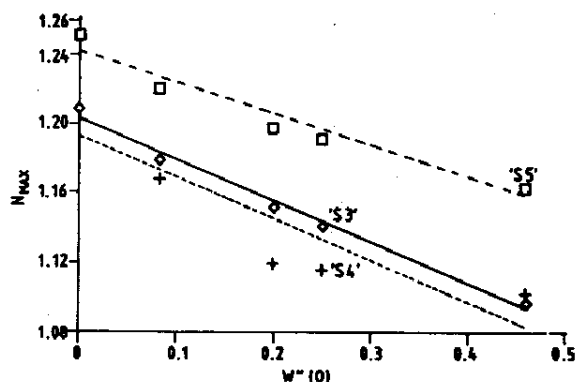


Figure 9. Maximum grey level (N_{max}) plot for test cases S3, S4 and S5.

- (b) Sharper filters were seemed to capture smaller features in the cross-sections. They also seemed to produce noisier images.
- (c) Despite discontinuities in the attenuation field in all of the test cases, the reconstruction error followed the analytical error estimates developed for smooth distribution.
- (d) Error magnitudes in all cases were uniformly small. This points towards the suitability of CBP for quantitative assessment of specimen cross-sections.

ACKNOWLEDGEMENTS

The authors are grateful to Shri Prahlada, Director, Defence Research & Development Laboratory (DRDL), Hyderabad, for the financial support given for this work. Useful discussions with Shri S.B. Kumar, Dr C. Muralidhar, Shri G.V. Siva Rao and Shri Sheri George are gratefully acknowledged.

REFERENCES

1. Davis, G. R.; Munshi, P. & Elliot, J. C. An analysis of biological hard tissues using the tomographic error formula. *J. X-ray Sci. Technol.*, 1996, 6, 63-76.

2. Herman, G. T. Image reconstruction from projections: The fundamentals of computerised tomography. Academic Press, New York, 1980.

3. Natterer, F. The mathematics of computerised tomography, John Wiley, New York, 1986.

4. Ramachandran, G. N. & Lakshminarayanan, A. V. Three-dimensional reconstruction from radiographs and electron micrographs: Application of convolution instead of Fourier transforms. *Proc. Natl. Sci. Acad., USA*, 1970, 68, 2236-240.

5. Munshi, P. Error Analysis of Tomographic Filters Part I: Theory. *NDT&E Internat.*, 1992, 25, 191-94.

6. Munshi, P.; Maisl, M. & Reiter, H. Experimental aspects of the approximate error formula for tomographic reconstruction. *Materials Evaluation*, 1997, 55(2), 188-91.

7. Wells, P. & Munshi, P. An investigation of the theoretical error in tomographic images. *Nucl. Instrum. Methods Phys. Res.*, 1993, 93, 87-92.